Local Layer Splitting: An Additive Manufacturing Method to Define the Mechanical Properties of Soft Pneumatic Actuators During Fabrication

Brice Parilusyan[1,2], Marc Teyssier[1], Zacharie Guillaume[1], Thibault Charlet[1], Clément Duhart[1] and Marcos Serrano[2]

***Abstract*— Additive manufacturing of silicone is increasingly being explored to complement the traditional molding fabrication technique for Soft Pneumatic Actuators (SPAs). However, the mechanical behavior of SPAs is defined by their 3D form, which leads to prioritizing the SPAs mechanical properties over their aspect. In this paper, we propose a novel SPA fabrication method where the mechanical properties of a silicone part are defined during the fabrication phase rather than the 3D modeling phase, leading to the object's mechanical properties being independent of the object's aspect. This novel SPA fabrication method, named Local Layer Splitting (LLS), consists of local modifications of the printing layer height to integrate stiffness variation, thus generating controlled mechanical deformation when pressured. We discovered that silicone printing layer height impacts the final stiffness of the material, and it could be used to program bending deformation to actuators during printing. We first characterize the effect of the layer height parameters on 3D-printed silicone stiffness with tensile tests. Then, we present a custom slicer we developed to generate G-codes with local layer height variations depending on the x and y positions. We then characterize the bending and force achievable by SPAs made with the LLS process and find that they match those of state-of-the-art SPAs. Finally, we present and discuss how the LLS method impacts the SPAs design by shifting the bending behavior integration from the SPAs 3D conception to their fabrication phase.**

I. Introduction

Additive Manufacturing (AM) of silicone is increasingly explored [1], [2] due to its multiple advantages. First, compared to the molding fabrication process, additive manufacturing allows for easier development of complex structures [3], [4], while reducing the number of fabrication steps [5]. Second, multi-extrusion additive manufacturing makes multi-material structures easily [6], [7]. Finally, the additive fabrication method offers a large set of unique fabrication characteristics (layer height, printing speed, temperature, infill, nozzle orientation) that can be modified to develop new mechanical and appearance features [8]. For these reasons, additive manufacturing is becoming an important fabrication method for soft robots, which tend to have a complex design and be made of multiple materials. [9], [10]

The additive manufacturing of soft pneumatic actuators (SPAs) is a 2-step process: The design of the SPA (which includes defining the SPA shape and 3D modeling it) and its Fabrication (which includes slicing the model and 3D printing it). The mechanical behaviors of inflated soft robots are usually controlled by design modifications, such as varying the dimensions and position of its cavities [5], or a stiffness variation of the SPA structure [11]. A change of these parameters implies a modification of the SPA 3D model, thus defining the mechanical properties of the actuator during the modeling step. Several structure modifications, such as cavities network integration in SPAs, lead to complex designs, especially for internal air chamber integration [2]. This constraint obliges prioritizing the SPA mechanical properties over its aspect, reducing the available SPA shapes, increasing their minimal size, and limiting new features integration such as sensors [12], [13].

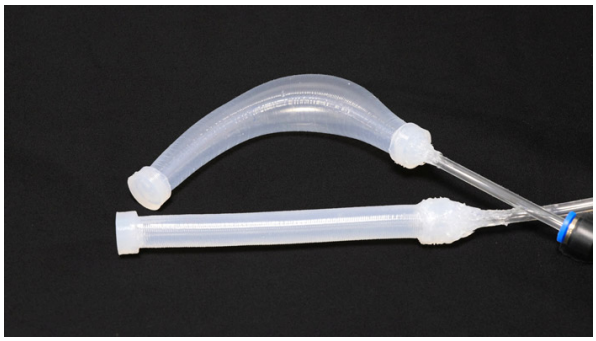

Fig. 1: 3D printed Soft Pneumatic Actuator using our LLS fabrication technique. (Bottom) The actuator shape is unaltered when non-pressurized. (Top) The actuator bends when pressurized.

Several methods exist to integrate mechanical deformations in SPAs without increasing the design complexity [14]. A wall thickness modification has a low impact on the overall design but reduces the mobility of the SPA and impacts its internal structure [15], [16]. Other approaches are to use multiple materials with different stiffness [10], [17], or to create specific machines capable of incorporating novel features such as rotational printing [18]. While these solutions lead to new designs and mechanical constraints, they severely increase the complexity of the fabrication process. We lack a method to print actuators with mechanical properties without impacting their aspect or increasing their fabrication complexity.

In this paper, we propose Local Layer Splitting (LLS), a novel method that uses a local variation in layer to define the mechanical properties of a silicone part during the fabrication phase rather than the modeling phase. With our approach, the object's mechanical properties become independent of the object's aspect. Our fabrication concept

*This work was supported by the french company Lynxter [19]

[1]Léonard de Vinci Pôle Universitaire, Research Center, France
[2]University of Toulouse 3, IRIT - Elipse, France

TABLE I: Printing parameters used with our custom slicer

Nozzle size (mm)	0.69	0.86	1.04
Bed temperature (C°)	70	80	80
Environment temperature (C°)	38	40	40
Printing speed (mm/s)	3	4	4
Infill (%)	0%	0%	0%
Retraction (mm/s)	1	1	1

is based on a local variation of layer height to create non-uniform anisotropic mechanical properties for SPAs. This process affects the stiffness of the printed silicone walls locally, directly impacting the mechanical deformation during material inflation. This technique controls the actuator's inflated geometry without impacting the overall aspect by integrating mechanical anisotropic properties in the silicone part. The SPAs modeled and fabricated with this method can integrate several bending properties in various directions, and these properties do not require a modification of the 3D model.

The main contributions of this paper are as follows:

- A novel SPA fabrication method based called Local Layer Splitting: local control of the layer height to create non-uniform anisotropic mechanical deformation.
- A universal extrusion-based slicer to generate G-code.
- An experimental characterization of the layer height impact on silicone stiffness.

We first introduce the working principles in Section II, which consists of an open-release slicer to generate non-uniform multiple-layer height G-codes, as well as the fabrication process of SPAs. Section III presents the mechanical characterization of the impact of the layer height on the stiffness of the 3D-printed silicone. Then we characterize the efficiency of SPAs fabricated with our LLS process in section IV. We present experimental evaluations of the bending and force abilities of the non-uniform anisotropic SPAs made with the LLS process. Next, we present a series of SPAs prototypes in section V to discuss future application opportunities. Finally, section VI concludes and presents future works on the LLS fabrication process.

II. Local Layer Splitting

This section introduces the Local Layer Splitting (LLS) fabrication method to create Soft Pneumatic Actuators (SPA) with non-uniform anisotropic mechanical properties. We present the general principle of LLS, then the slicing process, and finally, the materials used and the fabrication process.

A. General Principle

The traditional additive manufacturing process relies on the use of a set of constant parameters during the additive process e.g. layer height, thickness, temperature, infill, or printing speed. The printing process traditionally relies on 3D slicers that slice the 3D model vertically to generate G-CODE. The layer's parameters are constant and stack on each other successively, resulting in the printing nozzle moving up along the Z-axis only after each slice has been printed. Some

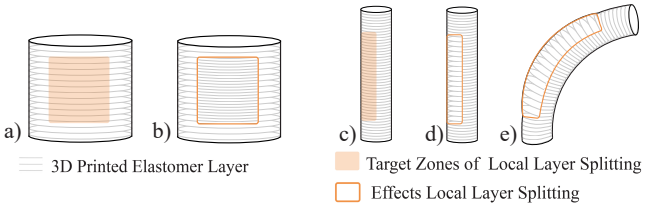

Fig. 2: Illustration of LLS technique. a) A 3D printed part, the orange area, is the target of LLS. b) The framed area shows the effect of LLS, leading to a different layer height. c) Cylindrical illustration of a SPA with a target zone of LLS d) The effect of LLS in the relaxed state and e) Shows the actuator in an inflated state.

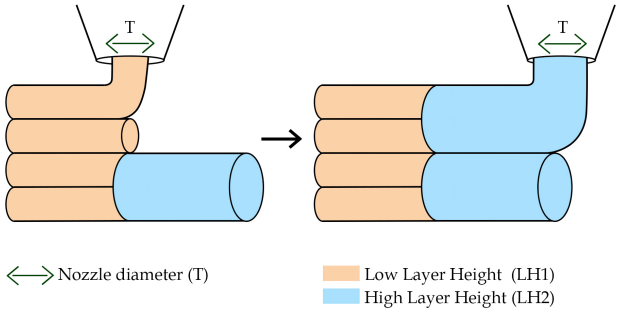

Fig. 3: Illustration of the 3D printing process of LLS. The Layer Height LH is correlated with the nozzle diameter T. the minimum layer height LH_1 and maximum layer height LH_2 are calculated as $LH_1 = \frac{1}{3}T$ and $LH_2 = \frac{2}{3}T$.

advanced slicers such as Cura or IceSL [19] can modify the layer height from one layer to another. However, these variations cannot apply to the same layer, the layer height remains constant and uniform over the entire layer.

Our LLS technique consists of slicing multiples area of the model using different layer height values. It results in a modification of the layer stack density in a local region of interest, as illustrated in Figure 2. The different layer stack density offers anisotropic mechanical properties in SPAs design during inflation.

B. Parametric Slicer Software

LLS requires changing the printing layer height according to the position on this layer over time, which is impossible on current mainframe extrusion-based slicers to our best knowledge. We developed a custom slicer to perform slicing with layer height variation at specific 3D locations of the model. The slicer is developed using the parametric modeling software Rhino's Grasshopper [20] and is inspired by *vase mode* printing (no infill, one sidewall). An SPA model designed in Rhino can be sliced with our software to incorporate several layer heights at specific locations of the model. Our software integrates basic printing parameters e.g. printing speed, extrusion factor, or wall thickness. The generated G-code is Reprap compatible, thus usable by

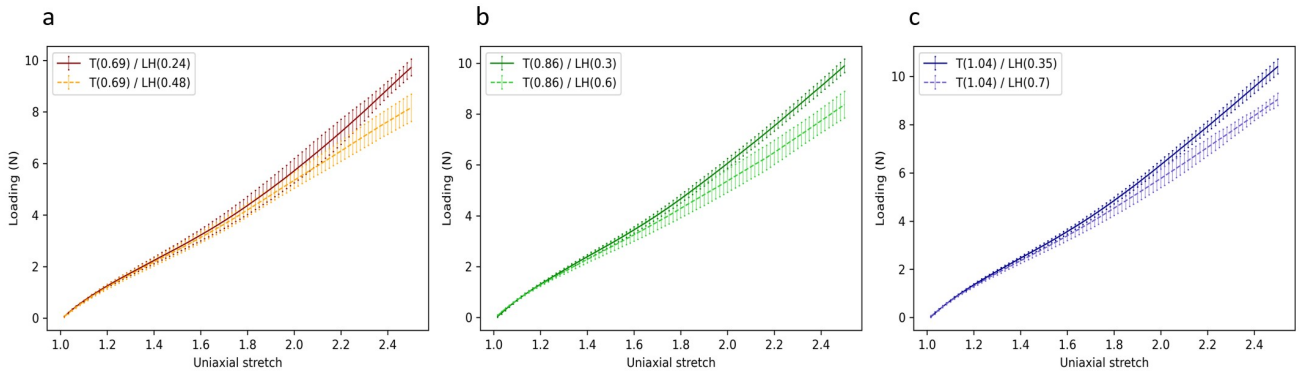

Fig. 4: Characterization result of the longitudinal force as a function of the sample elongation. Each graph represents a nozzle diameter T with a) Nozzle diameter $T = 0.69mm$. b) Nozzle diameter $T = 0.86mm$. c) Nozzle diameter $T = 1.04mm$; the biggest Layer Height LH of a T is drawn as a dotted line, and the thinner layer height is drawn as a straight line. The dotted line of any color is strictly below the straight line, demonstrating that a thinner LH increases the tensile stiffness of the material. We tested twelve samples for each curve.

all extrusion-based 3D printers. Our Grasshopper slicing program is available on Github[1].

C. Manufacturing Process

Wall numbers and their thickness impact the mechanical deformation from the LLS process. Consequently, each printed actuator is composed of one wall without infill. Silicone layer stacking is influenced by the silicone's reticulation time. Increasing temperature can speed up the cross-linking of bi-component silicone (platinum cured), thus speeding up the reticulation time. The actuators are printed standing to have a layer height variation along the actuator height direction. The top and bottom layers of the actuators are printed separately, then stuck to the SPAs using mono-component silicone.

In this paper, we printed the actuators on a Lynxter S600D 3D printer [21], a modular Extrusion Additive Manufacturing (EAM) printer with a controlled printing environment. The printing material used is the COP4025 silicone from COP [22], a 40 shore bi-component silicone skin-safe, with a reticulation time of 1 hour. The printer's controlled environment is heated to 40 degrees, and the printing speed is reduced to 6mm/s to achieve a successful print. We used three different nozzle sizes to extrude silicone, 0.69mm, 0.86mm, and 1.04mm. Table I shows the used printing parameters.

III. Material Characterization

This section evaluates the elongation properties of printed silicone based on LLS techniques according to the layer heights and with different thicknesses.

A. Parameters definition

Additive manufacturing is based on layer stacking; hence the layer height (LH) depends on the previous layer thickness (T). In our case, T is equivalent to the nozzle diameter. In thermoplastic 3D printing, the LH has to be lower than 75% of T and higher than 25% of T to ensure mechanical stability. As we use silicone, we relied on empirical evaluation to define the manufacturing limit of the layer height. We selected three nozzle sizes for all our experiments: 0.69mm, 0.86mm, and 1.04mm. Based on preliminary experimentation on our setup (printer, silicone, nozzle, and environmental conditions), we observed that LH has to be within $[\frac{1}{3}T; \frac{2}{3}T]$ to achieve a functional print, as presented in Fig. 3. For example, a nozzle diameter of 1.04mm will print a minimum LH of 0.35mm and a maximum LH of 0.7mm.

[1]https://local-layer-splitting.github.io/

B. Experimental Samples

Six types of samples were used for the tests. They were hand-cut from flat surfaces of vertically printed silicone actuators and had a standard dimension of 60mm by 5mm. We made twelve pairs of samples for each nozzle size (0.69mm, 0.86mm, 1.04mm) with their weight reported in table II.

C. Evaluation Protocol

We performed a mechanical tensile test to study the evolution of the sample elongation according to an applied force using a custom-made tensile testing machine with a load cell HX711 AD of 20kg. For each nozzle diameter (0.69mm, 0.86mm, 1.04mm), we measured the elongation for the two extreme samples (i.e. with dimensions of 60mm and 5mm). Every sample was pulled uni-axially up to a 150% stretching value, with stretching stress normal to the printing layers plane. From this test, the Young's modulus value of each sample is calculated using the formula 1

$$E = \frac{\sigma}{\epsilon} \tag{1}$$

The value σ is the stress calculated with the formula $\frac{F}{S}$ with F as the applied load and S as the sectional area. The value ϵ is the axial strain calculated with the formula $\frac{\Delta l}{l_0}$ with Δl as the elongation length and l_0 as the initial length.

D. Results & discussions

Fig. 4 plots the tensile test results for the layer height extreme of the three nozzle diameters. Each nozzle diameter curve has the same colors. We observe that, for a given T, the tensile stiffness is correlated to the LH of the sample. As a stronger tensile stiffness implies using a more significant load for equivalent stretching, these results show that an increase in layer height reduces the load used for stretching, thus reducing the tensile stiffness of the printed part. Also, we can see that this variation in tensile stiffness decreases while T increases. This means that an increase in the wall thickness T reduces the layer height impact on the tensile stiffness.

For example, doubling the layer height of the samples where $T = 0.69mm$ showed a Young's modulus of 16% (from 0.93 to 0.78), while for the samples where $T = 1.04mm$ it showed a Young's modulus of 13% (from 0.99 to 0.86).

TABLE II: Layer Height LH effect on material Young's modulus E for multiple nozzle diameters T at 250% stretch.

T (mm)	LH (mm)	Weight (g)	E (MPa)
0.69	0.24	0.64±0.025	0.93±0.03
0.69	0.46	0.64±0.022	0.78±0.05
0.86	0.3	0.65±0.032	0.94±0.02
0.86	0.6	0.65±0.021	0.8±0.05
1.04	0.35	0.67±0.018	0.99±0.03
1.04	0.7	0.66±0.012	0.86±0.05

IV. Evaluation of LLS application to SPAs

This section presents different experimental tests using Local Layer Splitting (LLS) to create two common Soft Pneumatic Actuators (SPA) with their corresponding characterization.

A. Experimental SPA Samples

We designed and printed one cylindrical shape SPA to be representative of the most common actuator designs. This actuator consists of a hollow tube (diameter = 10mm, height = 100mm). The cylindrical shape is standard for SPA and has no hard edges. All actuators are separated in half along the height with a LLS variation on each part. This design is printed using the three nozzle diameters T (0.69mm, 0.86mm, and 1.04). Each actuator are printed with two Layer Heights LH, the LLS variation depending on T as detailed in section III (LH minimum = $\frac{1}{3}T$ and LH maximum = $\frac{2}{3}T$).

B. Bending angles

Actuators' bending angles were defined as the angle from the base of the actuator to the center of the tip position. Pressurized air was applied up to 80 kPa using a valve and a precision compressor; the SPA angle was measured every 10 kPa. The bending angle was recorded using a camera and then calculated with movie editing software. We used five cylindrical actuators for this test.

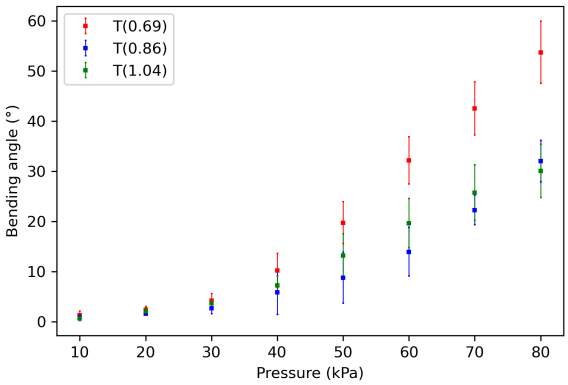

Fig. 5: Measure of the bending angle as a function of the applied internal air pressure for cylindrical SPAs. The measure of the actuator was stopped when they reached the end of their elastic deformation potential: around 80kPa for T = 0.69mm, T = 0.86mm and T = 1.04mm. We experimented with five samples.

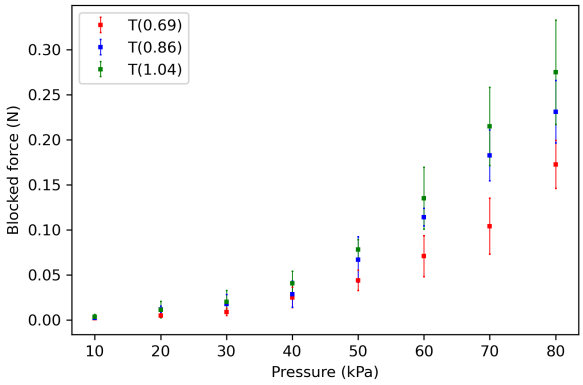

Fig. 6: Blocked force as a function of the applied internal air pressure for cylindrical SPAs. The SPAs blocked force is consistent with their bending angle. The measure of the actuator was stopped when it reached 80kPa. A maximum blocked force of 0.36N was observed for the nozzle diameter T = 1.04mm. We experimented with five samples.

Fig. 5 plots the bending angle of the cylindrical SPAs as a function of the applied pressure. An increase in the bending angle can be measured when the applied pressure increases. This result validates that the LLS process induces local anisotropic mechanical properties, which can be used to integrate mechanical deformation for SPAs when pressured. The maximum bending angle obtained is 60.8° for an 80 kPa pressure; this result was obtained with the 0.69mm thick SPA before entering plastic deformation. This bending value corresponds to state-of-the-art SPAs bending value with a higher pressure level due to the high shore of the material used (shore 40). Finally, results showed that the nozzle diameter T affects the bending potential of the SPAs.

Fig. 7: Example of multiple bending SPAs made with the LLS method. The SPA nozzle diameter is T = 0.86mm, and each side of the actuator has a different layer height value. These values are swapped at half of the actuator, which results in a two-directional bending.

C. Blocked force

The actuator's blocked force was calculated using a load cell placed in the direction of the actuator tip during actuation. We used five cylindrical actuators with the same characteristics as the bending angle test. Pressurized air was applied up to 80 kPa using a valve and a compressor, and the SPA blocked force was measured every 10 kPa. Figure 6 plots the bending angle of the SPAs as a function of the applied pressure. Results show that the maximal force achieved of 0.36 N comes from the thickest nozzle diameter T = 1.04mm. The force curve is not linear, and significant strength appears above 50kPa. After 80kPa the actuators have a reduction in blocked force. It may happen because the actuator reaches its bending deformation limit and expands in size and length. This results in a low increase of the blocked force from the bending. We also observed that above 80kPa, the SPAs deformation becomes permanent as they reach their plastic deformation domain.

V. Applications and Discussion

A. Applications

We designed two examples to illustrate our Local Layer Splitting (LLS) technique. The first one consists of a three-finger gripper shown in Figure 8. This gripper is made from three cylinder-shaped SPA. We tried to design a human-inspired gripper with two fingers and a thumb. For the fingers, we used SPAs with a nozzle diameter T = 0.86mm, and for the thumb, we used a SPA with a T = 0.69mm. As shown in section IV, the T=0.69mm SPA can deploy more strength than the others, thus simulating a thumb. We performed grasping tests on objects of different sizes and shapes; a polyester egg (8.6g), a USB key (25.4g), and a cardboard miniature (36.7g).

The second example illustrated in Fig. 7 demonstrates the complex mechanical possibilities of the LLS process. We designed an actuator (diameter = 10mm, height = 120mm) with multiple bendings defined using the LLS fabrication method. The nozzle diameter T is 0.86mm, and the layer heights LH are 0.3mm and 0.6mm. We integrated multiples area with the smaller layer height (0.3mm) to generate multiple bending behaviors when pressured. This example demonstrates that a single SPA can have different anisotropic properties at different locations by using the LLS method. This fabrication method allows easy customization of the bending behavior by increasing the number of LLS areas and their dimension on the SPA.

B. Discussion

The traditional mold-based SPA manufacturing process is incompatible with iterative design. This manufacturing process involves various fabrication steps and the creation of unique molds for a given SPA design. One main advantage of LLS is that the mechanical properties are not linked to the SPA design but to its manufacturing process. Precedent examples illustrate how the LLS technique can be used to separate the SPA model design from its mechanical properties. These properties are defined during the SPA manufacturing. This separation allows a single SPA design to generate an unlimited quantity of achievable bending behaviors.

The LLS technique opens up new opportunities for SPA design. First, this technique provides a straightforward solution to add local anisotropic properties for pneumatic deformation. Second, our approach is fully automated, saving manufacturing time and reducing errors during the manufacturing process. Finally, updating and iterating on the deformation behavior of an actuator can be made quickly. In opposition to the solutions proposed in the literature [5], our method does not require any modification of the initial SPA model design. This independence of the mechanical properties from the object's aspect allows for the exploration of new SPA designs.

VI. Conclusion and Future Work

A. Conclusion

Soft Pneumatic Actuators are increasingly manufactured with 3D printers. In this paper, we take advantage of the layer height effect on the stiffness of the 3D-printed silicone and propose a method to program the local mechanical deformation of SPAs during their fabrication while maintaining the actuator's shape. Our method, named "Local Layer Splitting" (LLS), relies on a variation of the layer height on a specific 3D area of the SPA model, creating local variations of the mechanical properties of the SPA and impacting the SPA shape when inflated. This process relies only on a dynamic tuning of printing parameters to modify the bending deformation and strength without changing the SPA design. We characterized the maximum bending and force achievable by the SPAs made with LLS. Our SPAs achieved a maximum bending angle of 60.8° with a pressure of 80kPa. Furthermore, our experimental results reveal how the layer height and nozzle diameter impact mechanical deformation. To sum up, LLS is a new opportunity for SPAs fabrication that allows quick and easy customization of the bending behavior. Its automation with a 3D printer allows better control of mechanical deformation. The LLS process can impact the traditional design of SPAs by shifting the

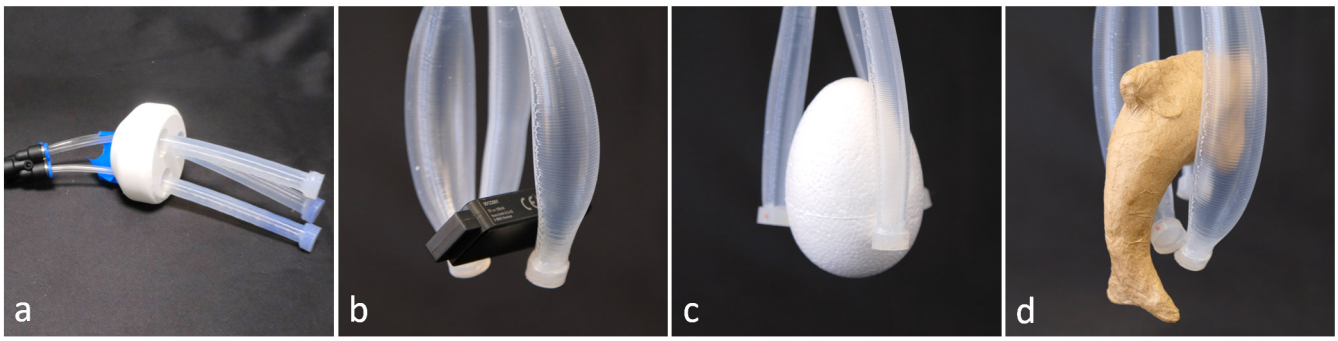

Fig. 8: Three-finger gripper grasping test. (a) Two fingers have a nozzle diameter T = 0.86mm and the last T = 0.69mm to deliver increased strength, thus simulating a thumb. The gripper demonstrated his handling potential of objects; (b) a USB key (25.4g), (c) a polyester egg (8.6g), and a cardboard miniature (36.7g).

integration of bending behaviors from the model design to its fabrication.

B. Future work

The experiments presented in this paper mainly explore the control of layer height. However, other additive manufacturing control parameters could be explored more deeply such as printing orientation [23], infill [24], or temperature [15].

Future tests are planned to characterize the effects of the SPAs shape more precisely to understand the link between the layer height variation, printed surface, model volume, and bending angle. The printing temperature should also be explored to understand its impact on the SPA mechanical properties. We plan to characterize bending with several layer height ratios and wall thickness. This characterization will automatically generate the Local Layer Splitting (LLS) parameters to apply to the SPA in the desired angle.

Our current custom slicer requires having the SPA designed in Grasshopper. This might impact the ease of use and design freedom. The next step towards the democratization of the LLS technique is to improve our slicer to provide user-friendly software and algorithm, thus simplifying the customization of SPAs. Finally, we would like to explore other SPAs shapes and mix the LLS fabrication process with an infill variation.

VII. Acknowledgment

This work was supported by an industrial research partnership with Lynxter [21]. The authors would like to thank the company for the help provided.

References

[1] C. Tawk and G. Alici, "A review of 3d-printable soft pneumatic actuators and sensors: Research challenges and opportunities," Advanced Intelligent Systems, vol. 3, no. 6, p. 2000223, 2021.

[2] J. M. Florez, B. Shih, Y. Bai, and J. K. Paik, "Soft pneumatic actuators for legged locomotion," in 2014 IEEE International Conference on Robotics and Biomimetics (ROBIO 2014). IEEE, 2014, pp. 27–34.

[3] W. Hu, W. Li, and G. Alici, "3d printed helical soft pneumatic actuators," in 2018 IEEE/ASME International Conference on Advanced Intelligent Mechatronics (AIM). IEEE, 2018, pp. 950–955.

[4] C. Tawk, E. Sariyildiz, H. Zhou, M. in het Panhuis, G. M. Spinks, and G. Alici, "Position control of a 3d printed soft finger with integrated soft pneumatic sensing chambers," in 2020 3rd IEEE International Conference on Soft Robotics (RoboSoft). IEEE, 2020, pp. 446–451.

[5] A. Altelbani, H. Zhou, S. Mehrdad, F. Alambeigi, and S. F. Atashzar, "Design, fabrication, and validation of a new family of 3d-printable structurally-programmable actuators for soft robotics," IEEE Robotics and Automation Letters, vol. 6, no. 4, pp. 7941–7948, 2021.

[6] M. A. Skylar-Scott, J. Mueller, C. W. Visser, and J. A. Lewis, "Voxelated soft matter via multimaterial multinozzle 3d printing," Nature, vol. 575, no. 7782, pp. 330–335, 2019.

[7] A. Miriyev, B. Xia, J. C. Joseph, and H. Lipson, "Additive manufacturing of silicone composites for soft actuation," 3D Printing and Additive Manufacturing, vol. 6, no. 6, pp. 309–318, 2019.

[8] O. D. Yirmibesoglu, J. Morrow, S. Walker, W. Gosrich, R. Cañizares, H. Kim, U. Daalkhaijav, C. Fleming, C. Branyan, and Y. Menguc, "Direct 3d printing of silicone elastomer soft robots and their performance comparison with molded counterparts," in 2018 IEEE International Conference on Soft Robotics (RoboSoft). IEEE, 2018, pp. 295–302.

[9] T. Hainsworth, L. Smith, S. Alexander, and R. MacCurdy, "A fabrication free, 3d printed, multi-material, self-sensing soft actuator," IEEE Robotics and Automation Letters, vol. 5, no. 3, pp. 4118–4125, 2020.

[10] T. Calais, N. D. Sanandiya, S. Jain, E. V. Kanhere, S. Kumar, R. C.-H. Yeow, and P. Valdivia y Alvarado, "Freeform liquid 3d printing of soft functional components for soft robotics," ACS Applied Materials & Interfaces, vol. 14, no. 1, pp. 2301–2315, 2021.

[11] J. I. Lipton and H. Lipson, "3d printing variable stiffness foams using viscous thread instability," Scientific reports, vol. 6, no. 1, pp. 1–6, 2016.

[12] R. L. Truby, R. K. Katzschmann, J. A. Lewis, and D. Rus, "Soft robotic fingers with embedded ionogel sensors and discrete actuation modes for somatosensitive manipulation," in 2019 2nd IEEE International Conference on Soft Robotics (RoboSoft). IEEE, 2019, pp. 322–329.

[13] F. Spina, A. Pouryazdan, J. C. Costa, L. P. Cuspinera, and N. Münzenrieder, "Directly 3d-printed monolithic soft robotic gripper with liquid metal microchannels for tactile sensing," Flexible and Printed Electronics, vol. 4, no. 3, p. 035001, 2019.

[14] J. Chen, X. Liu, Y. Tian, W. Zhu, C. Yan, Y. Shi, L. B. Kong, H. J. Qi, and K. Zhou, "3d-printed anisotropic polymer materials for functional applications," Advanced Materials, vol. 34, no. 5, p. 2102877, 2022.

[15] A. Firouzeh, M. Salerno, and J. Paik, "Soft pneumatic actuator with adjustable stiffness layers for multi-dof actuation," in 2015 IEEE/RSJ International Conference on Intelligent Robots and Systems (IROS). IEEE, 2015, pp. 1117–1124.

[16] U. Yoo, Y. Liu, A. D. Deshpande, and F. Alamabeigi, "Analytical design of a pneumatic elastomer robot with deterministically adjusted stiffness," IEEE Robotics and Automation Letters, vol. 6, no. 4, pp. 7773–7780, 2021.

[17] R. L. Truby, M. Wehner, A. K. Grosskopf, D. M. Vogt, S. G. Uzel, R. J. Wood, and J. A. Lewis, "Soft somatosensitive actuators via embedded 3d printing," Advanced Materials, vol. 30, no. 15, p. 1706383, 2018.

[18] N. M. Larson, J. Mueller, A. Chortos, Z. S. Davidson, D. R. Clarke, and J. A. Lewis, "Rotational multimaterial printing of filaments with subvoxel control," Nature, pp. 1–7, 2023.

[19] IceSL, "Advanced slicing software for 3d printing research." [Online]. Available: https://icesl.loria.fr/#header

[20] Grasshopper, "Rhino, 3d modeling software." [Online]. Available: https://www.rhino3d.com/fr/6/new/grasshopper/

[21] Lynxter, “3d printer manufacturer.” [Online]. Available: https://lynxter.fr/en/
[22] COP, “Creative and responsible chemistry.” [Online]. Available: https://www.cop-chimie.com/fr/produit/copsil-3d-4025-2/
[23] L. Garcia, M. Naves, and D. M. Brouwer, “3d-printed flexure-based finger joints for anthropomorphic hands,” in 2018 IEEE/RSJ International Conference on Intelligent Robots and Systems (IROS). IEEE, 2018, pp. 1437–1442.
[24] M. Fernandez-Vicente, W. Calle, S. Ferrandiz, and A. Conejero, “Effect of infill parameters on tensile mechanical behavior in desktop 3d printing,” 3D printing and additive manufacturing, vol. 3, no. 3, pp. 183–192, 2016.